energies

MDPI

Article

Ab-Initio Molecular Dynamics Simulation of the Electrolysis of Nucleobases

Irmgard Frank [1,*] and Ebrahim Nadimi [1,2]

[1] Theoretische Chemie, Universität Hannover, Callinstr. 3A, 30167 Hannover, Germany; nadimi@kntu.ac.ir
[2] Faculty of Electrical Engineering, K. N. Toosi University of Technology, P.O. Box 16315-1355, Tehran 1996715433, Iran
* Correspondence: irmgard.frank@theochem.uni-hannover.de

Abstract: Electrolysis is potentially a valuable tool for cleansing waste water. One might even hope that it is possible to synthesize valuable products in this way. The question is how the reaction conditions can be chosen to obtain desired compounds. In the present study we use Car–Parrinello molecular dynamics to simulate the reaction of nucleobases under electrolytic conditions. We use our own scheme (F. Hofbauer, I. Frank, Chem. Eur. J., 18, 277, 2012) for simulating the conditions after the electron transfer in a self-consistent field calculation. This scheme was employed previously to the electrolysis of pure water and of polluted solutions. On the picosecond timescale, we find a strongly different reaction behavior for each of the four nucleobases contained in DNA.

Keywords: Car–Parrinello molecular dynamics; electrochemistry; reaction intermediates; reaction mechanisms

Citation: Frank, I.; Nadimi, E. Ab-Initio Molecular Dynamics Simulation of the Electrolysis of Nucleobases. *Energies* **2021**, *14*, 5021. https://doi.org/10.3390/en14165021

Academic Editor: Jin-Soo Park

Received: 24 June 2021
Accepted: 12 August 2021
Published: 16 August 2021

1. Introduction

Two billion people have no access to clean toilets. Having clean toilets is not possible without clean water. In certain situations water is rare in contrast to electric current. This applies to arid regions on Earth but also to the situation in the international space station (ISS). It is necessary to have closed circuits which involve fast and efficient cleansing of waste water. Cleansing waste water is possible by various means. After filtration and biochemical processes it still contains bioorganic compounds. Nanofiltration with pores of about 2 nm can change that to some degree. Compounds like amino acids and nucleobases have a size of about 1 nm, hence even with nanofiltration they are not completely removed. The same is true for compounds like urea and uric acid which we investigated previously [1]. Electrolysis might help to remove such undesired compounds from a solution. It is even possible that valuable products are formed by electrolysis such as molecular hydrogen. In the present paper we investigate the fate of nucleobases. The experimental interest in the electrochemistry of nucleobases is old [2,3], but there are also more recent publications which typically describe more complex systems [4,5]. For simulating electrolytic reactions, we use our established scheme for simulating the situation near an electrode (Figure 1, see also [1,6,7]).

In this scheme we consider the situation after mass transport of positively/negatively charged species towards the negatively/positively charged electrodes and discharging of these species near the electrode. We simulate anodic and cathodic reactions separately which is justified by the fact that, seen at the nanometer scale, the two electrodes are far away from each other. After the mass transport, the chemical situation is clearly different for anodic and cathodic space. Near the anode OH^- ions are discharged. Hence we simulate the situation of an aqueous liquid containing a pollutant by removing 4 H^+ ions and 4 electrons e^- from 4 water molecules in the mixture. Close to the cathode, H^+ or H_3O^+ is discharged. Here we remove 4 OH^- ions and add four electrons. Alternatively, one could have added four H^+ ions and four electrons. The numbers are chosen in a way

to observe reactions soon without too high concentrations of $OH^{\cdot}$ or $H^{\cdot}$ radicals; see also the Methods section.

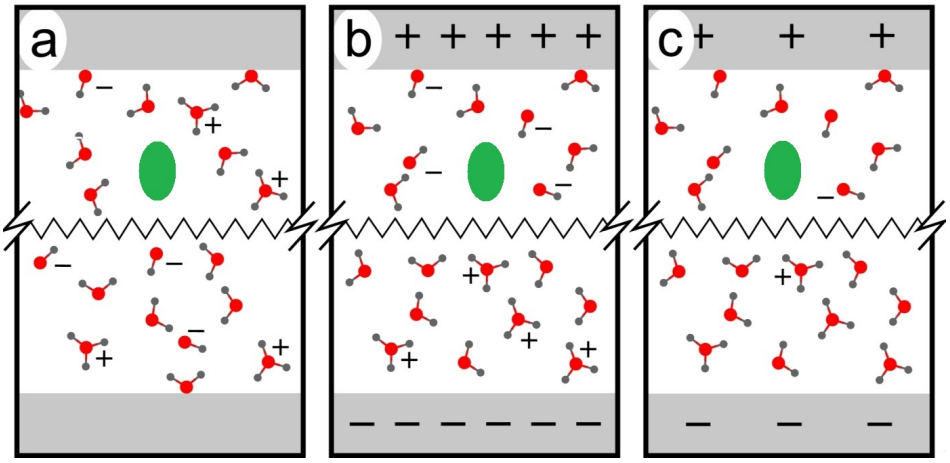

Figure 1. General model: We consider an aqueous solution containing a pollutant (green). (**a**) The situation before applying a potential is stable. The solution contains a small amount of OH^- and H_3O^+ molecules (in a much smaller concentration than shown here). (**b**) If a potential is applied there is a mass transport of the OH^- ions to the anode and of the H_3O^+ ions to the cathode. The same accounts for other charged species which may be formed during the reaction. (**c**) Close to the electrode surfaces, the ions are discharged. Due to electronic tunneling, a direct contact to the electrode is not necessarily needed. As a result, we have a pollutant in contact with radicals and with water. We take this as the starting point of our simulations.

Our procedure is different from other approaches [8–10]. It resembles the approach we are using when simulating photoreactions [11]: there we equilibrate the system in the ground state, then switch instantaneously to the excited state and let it go. This means that we have no reliable way to describe phenomena like the excitation itself on the attosecond timescale. We rather see what is properly called photochemistry, that is, the breaking and formation of chemical bonds. In addition, in the case of electrochemistry we instanteneously change the composition. We do not make an attempt to simulate the electron transfer itself, which is difficult in a reproducible way if using a self-consistent field (SCF) approach. Furthermore, we apply no external field. This is justified by the fact that we compute very small systems ($\approx$1 nm^3), and at this scale the potential difference is negligible. We focus on the chemistry triggered by the instantaneous electron transfer. For the simulations we use the Car–Parrinello molecular dynamics code [12,13] with the BLYP functional [14]; for details see the Methods section.

Starting in the vast field of the rich nucleobase electrochemistry, we want to keep things as simple and elementary as possible. Hence, in the present study, we simulate the electrochemistry of the nucleobases in water. Further steps will be the addition of an electrolyte and maybe also of an electrode and/or a heterogeneous catalyst. Ideally the electrode does not undergo chemical reactions, but there might be to some degree also surface catalysis which is different from a purely electronic catalysis.

2. Results and Discussion

2.1. Adenine

We start with adenine (compound **1**, Figure 2). The observed reaction mechanisms have some properties in common for the anodic and the cathodic reactions. In both cases we observe no ring opening. The hydrogen atom connected to the six-membered ring is never attacked. The same is true for the hydrogen atom connected to the five-membered ring. We observe several reaction products, see Figure 2. The compounds **1a** and **1b** are formed by the simple abstraction of hydrogen atoms from adenine. OH radicals are the active moieties. By abstraction of hydrogen, they are transformed into stable water

molecules. An alternative reaction is the addition of an OH radical, leading to compound **1c**. All these reactions of OH radicals which occur at the anode are strongly determined by the initial geometry. A more interesting reaction product is compound **1d**, which is formed at the cathode in three of eight simulations. It represents a less stable isomer of adenine (BLYP: 7.3 kcal/mol, B3LYP: 8.4 kcal/mol). The mechanism is described in Figures 3 and 4. Figure 3 demonstrates how this reaction is connected with the formation of molecular hydrogen. It is possible with little motion of the nuclei. Figure 4 shows the change of single coordinates. The H_2 formation is the driving force for the formation of a less stable isomer.

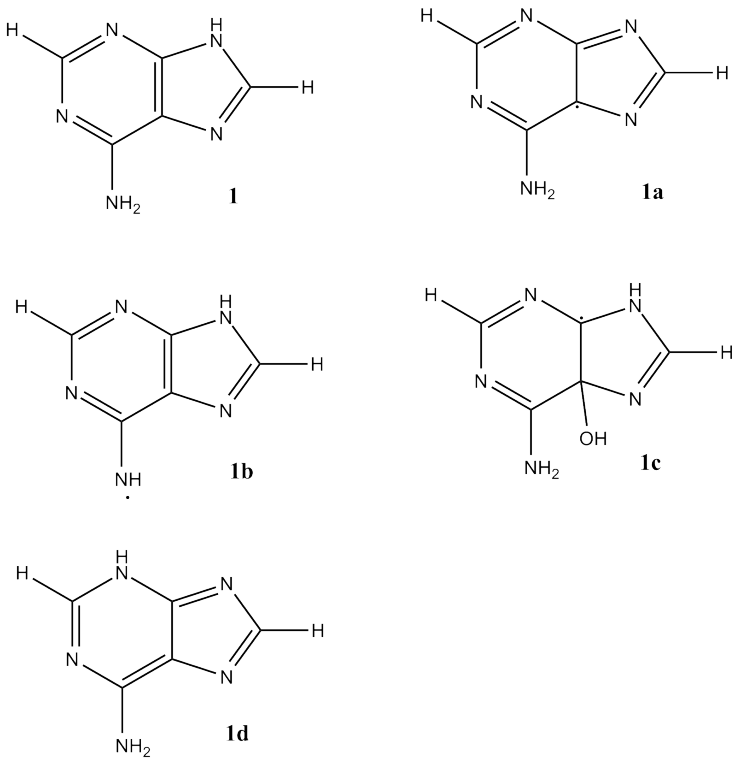

Figure 2. Reaction products of the electrolysis of adenine **1**. Anodic reaction: **1a**, **1b**, and **1c**, cathodic reaction: **1d**.

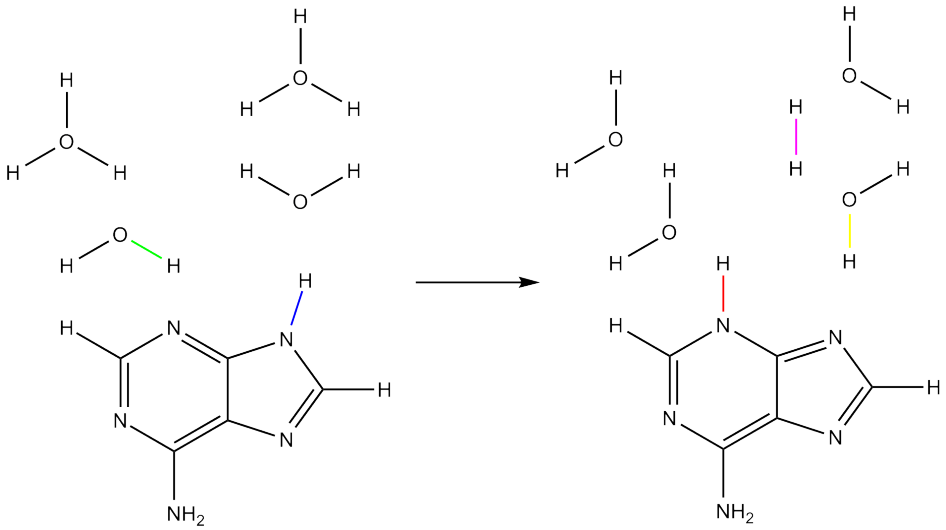

Figure 3. Reaction mechanism which leads to the formation of the adenine isomer **1d** which was exclusively observed under cathodic conditions. The oxidation state of the adenine moiety stays the same, but a H_2 molecule is formed.

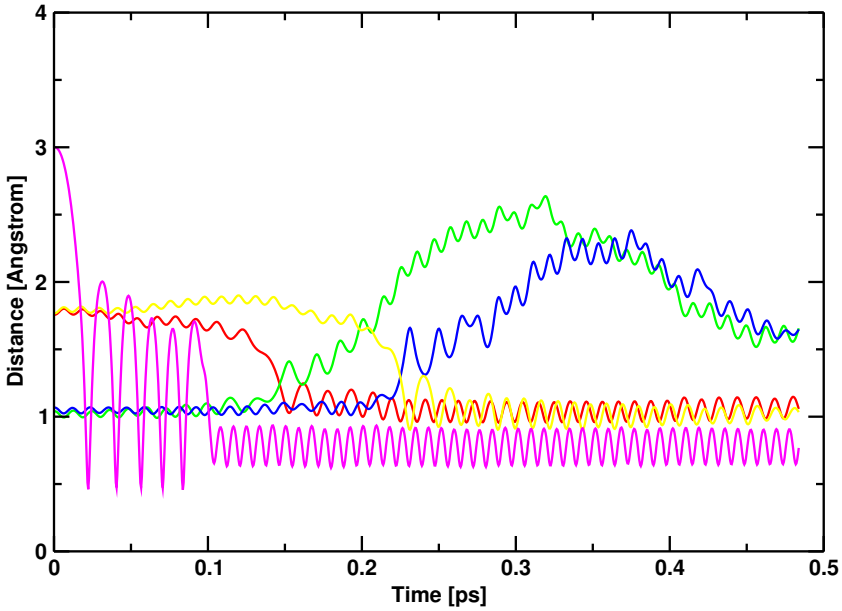

Figure 4. Formation of **1d**: Change of distances with time, compare to Figure 3. Green and blue: bonds that are broken. Magenta, red and yellow: bonds that are formed. Initially, molecular hydrogen is formed. The reaction continues with the formation of the N-H bond marked in red. Almost simultaneously the O-H bond marked in green is broken. The breaking of the second N-H bond and the formation of the second O-H bond occur about 0.1 ps later.

2.2. Cytosine

Cytosine (**2**, Figure 5) showed almost no reactivity at the cathodic side, while interesting products were formed under anodic conditions. Again, the rings were not broken. In addition, like for adenine, some parts of the structure are relatively stable, in particular the CO double bond and the CC double bond. The latter is attacked only in one case which leads to formation of compound **2c**. Compounds **2a** and **2b** are formed by simple hydrogen abstraction, compound **2d** by OH addition. Compound **2e** was formed at the cathodic side by addition of nascent hydrogen. Its formation is strongly dependent on the initial geometry; normally cytosine is stable under cathodic conditions. The most interesting product is compound **2f**. After anodic hydrogen abstraction, dimerization is possible. This result was observed in two out of eight simulations. Nevertheless, as it was observed immediately after discharging, its formation was strongly dependent on the initial geometry (Figures 6 and 7). The abstraction of two hydrogen atoms by two OH radicals is complete after 0.05 ps. The formation of the N-N bond occurs about 0.1 ps later (Figures 7 and 8). A movie of the reaction, showing also the spin densities, is available in the Supplementary Material. Remarkably, during the reaction, almost no spin densities are observed, hence almost all electrons succeed in being paired during this reaction. This is in contrast to what we observed for other compounds [1,6].

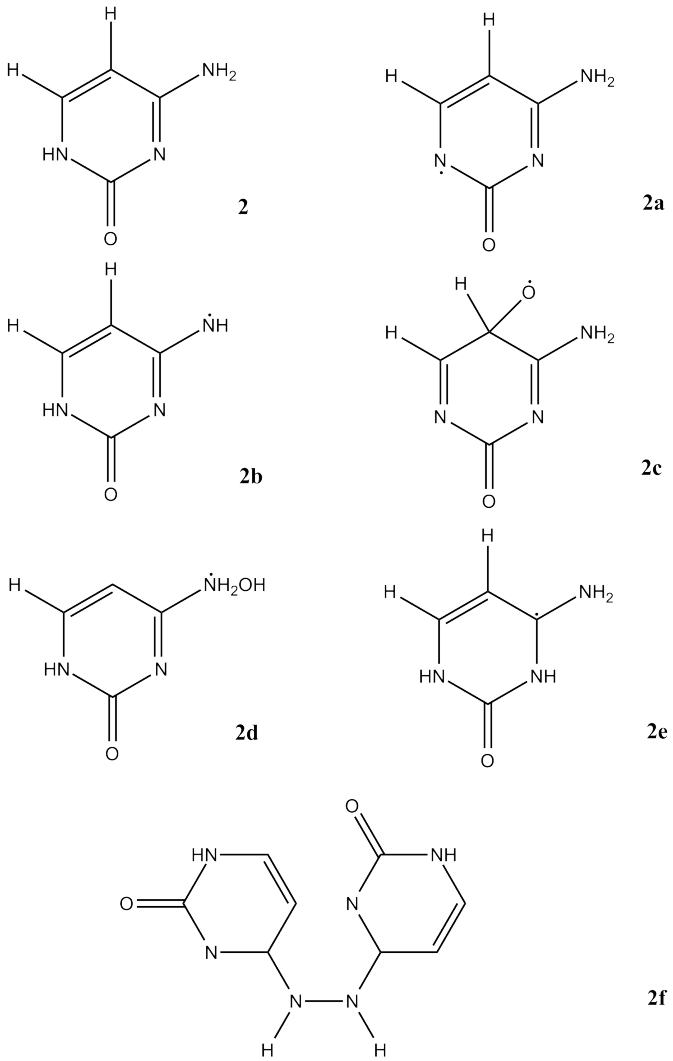

Figure 5. Reaction products of the electrolysis of cytosine **2**. **2e** was the only reaction product observed in the cathodic space.

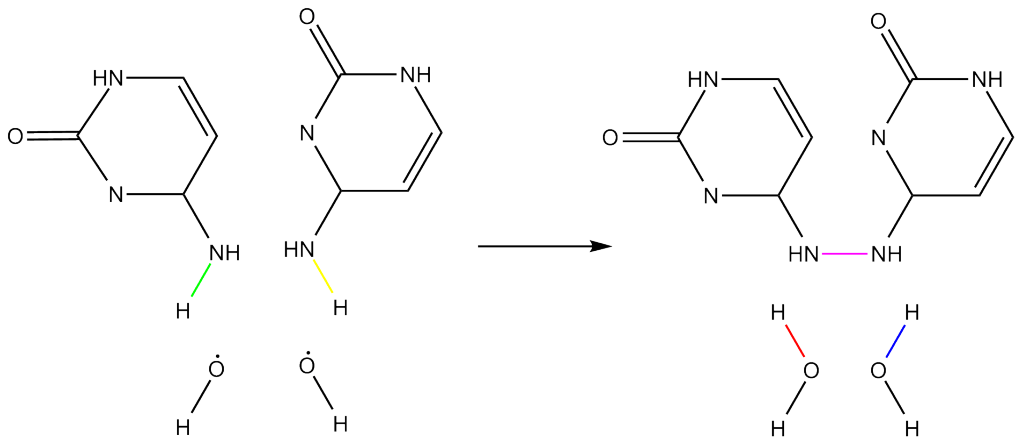

Figure 6. Reaction mechanism which leads to the formation of **2f**.

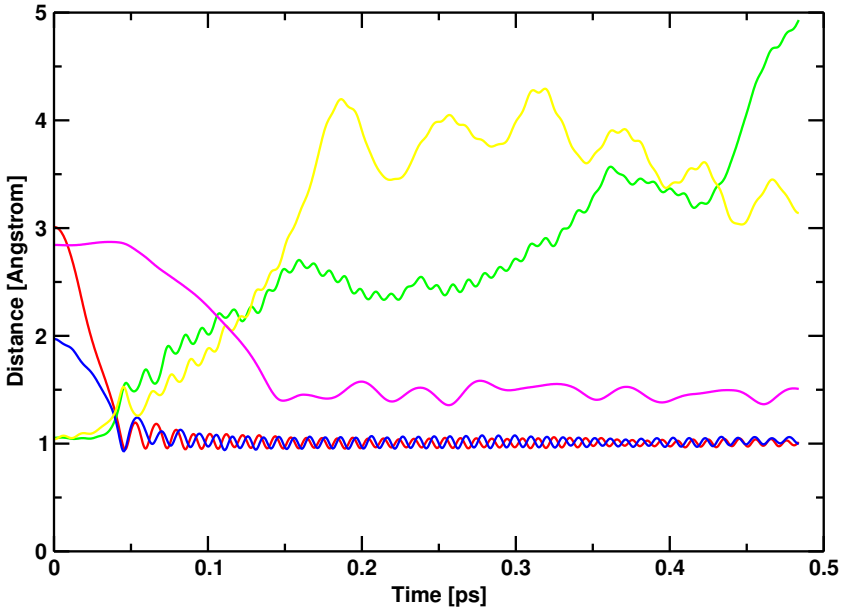

Figure 7. Formation of **2f**: Change of distances with time, compare to Figure 6. Green and yellow: bonds that are broken. Red, blue and magenta: bonds that are formed.

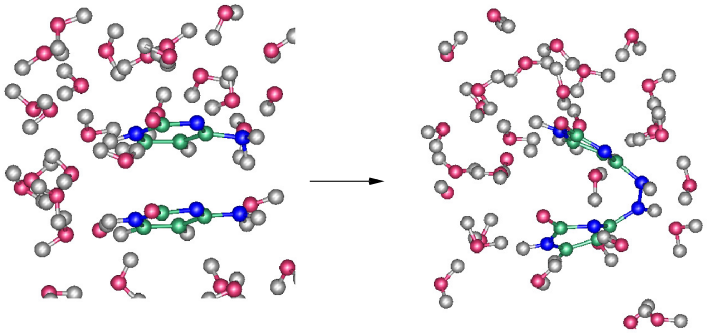

Figure 8. Formation of **2f**: Dimerization.

2.3. Guanine

Electrolysis of guanine **3** leads to a variety of interesting products (Figure 9). **3a** is formed near the anode by simple hydrogen abstraction of the OH radical. It is also observed, however, near the cathode by hydrogen abstraction of nascent hydrogen. The products **3b**–**3e** stem from several reaction steps, which, in the anodic space, always consist of hydrogen abstraction and OH addition. **3g** is the result of two isomerization reactions at the cathode. Finally, we observe a ring-opening reaction leading to **3f**. Figures 10 and 11 illustrate the reaction mechanism for this ring opening. It is started by two abstraction reactions in which OH radicals take two hydrogen atoms from the ring system. This unstable situation is stabilized about 0.1 ps later by the addition of a third OH radical which again leads to the opening of the ring about 0.3 ps after the start of the reaction.

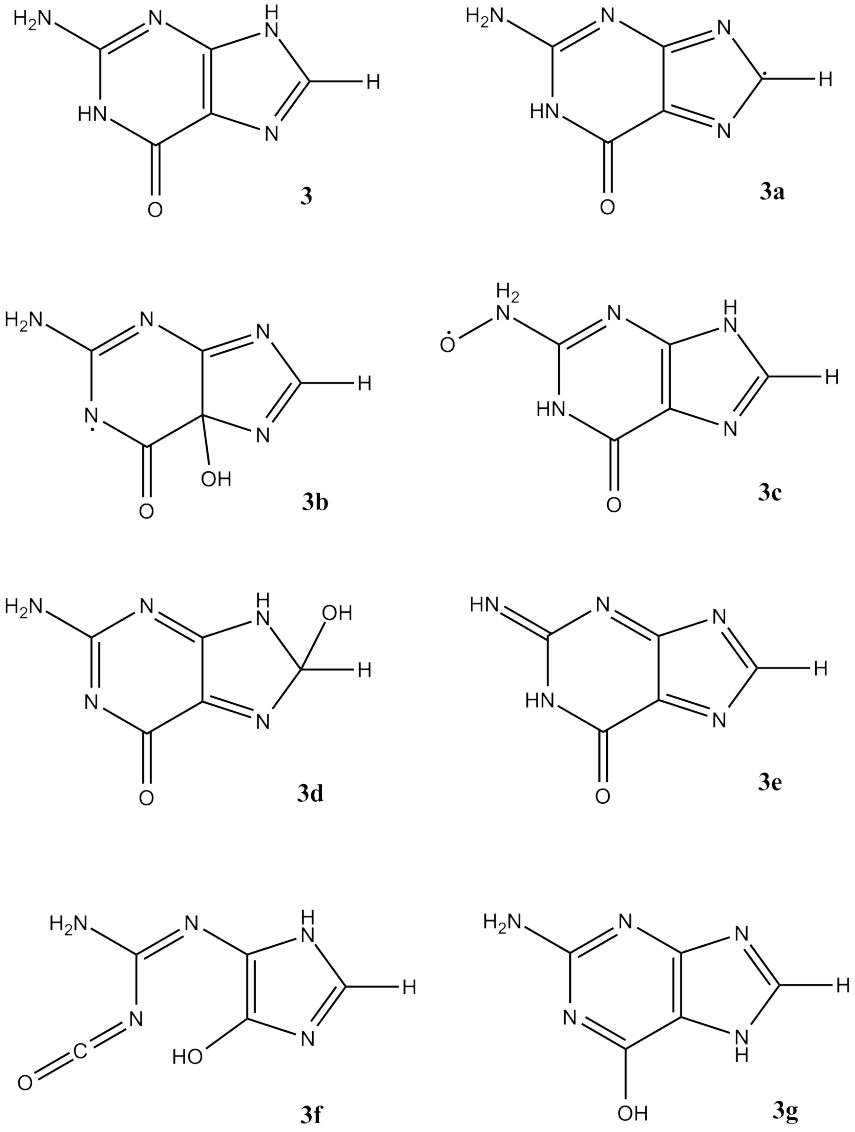

Figure 9. Reaction products of the electrolysis of guanine **3**. **3b**–**3f**: Reaction products at the anode. **3g** was observed at the cathode, **3a** near both electrodes.

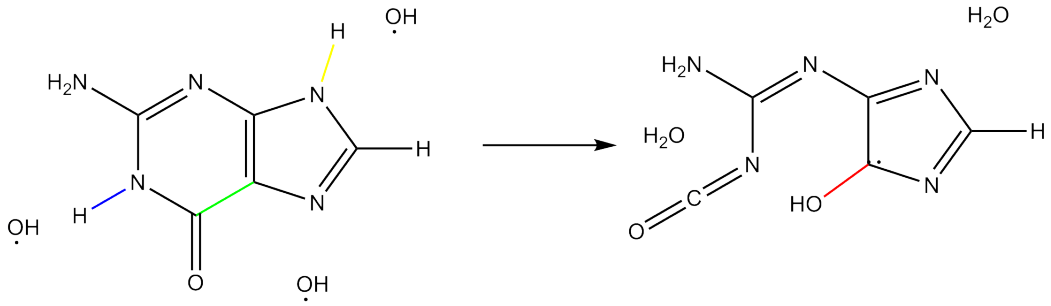

Figure 10. Reaction mechanism which leads to the formation of **3f**.

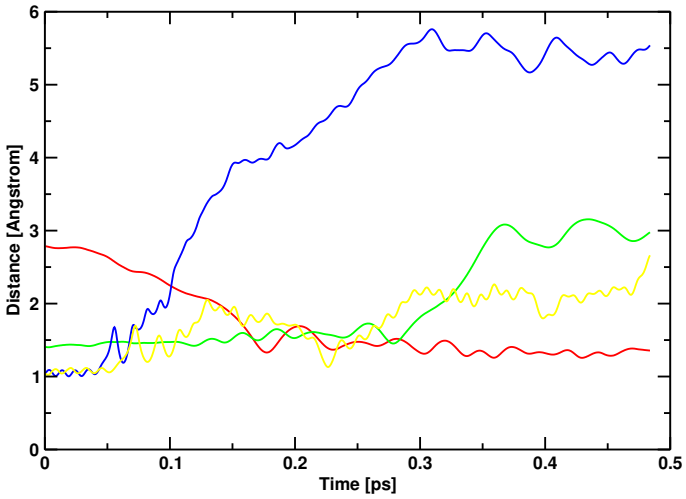

Figure 11. Formation of **3f**: Change of distances with time, compare to Figure 10. Blue, green and yellow: bonds that are broken. Red: bond that is formed.

2.4. Thymine

Electrolysis of thymine **4** led to several products without a clear pattern (Figure 12). Again, the single reaction steps are simple hydrogen abstractions or OH additions. Except in the case of **4f**, where the methyl group is oxidized, the resulting molecules are unstable radicals and are rather intermediates than products.

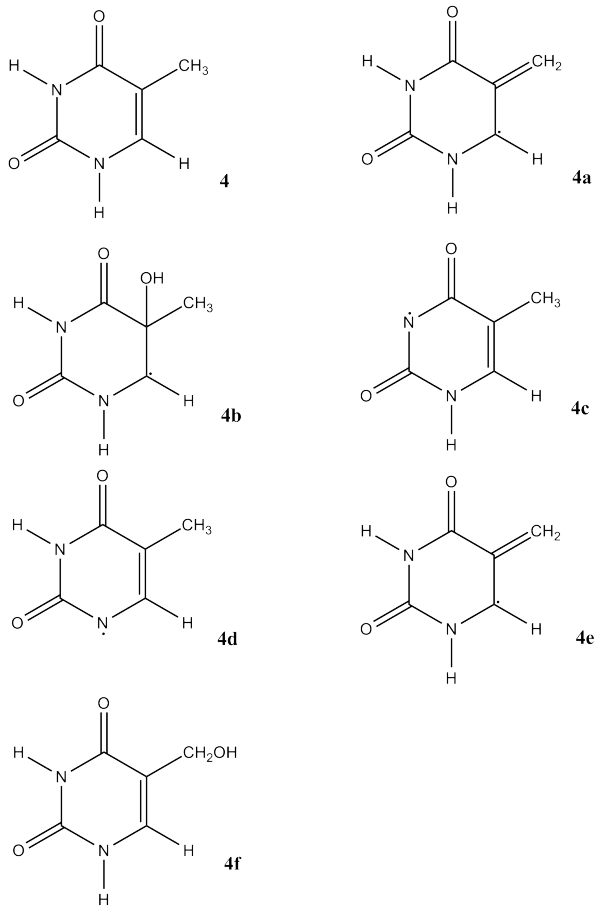

Figure 12. Reaction products of the electrolysis of thymine **4**. All these products were observed near the anode. **4c** was observed near both electrodes.

2.5. Energetics

The energy changes connected with the most important pathways are listed in Table 1, as computed with Hartree–Fock, post-Hartree–Fock and DFT methods [14–17].

Table 1. Reaction energies in kcal/mol computed with Hartree–Fock, post-Hartree–Fock and DFT methods.

Reaction	HF	MP2	CCSD	BLYP	B3LYP	B2PLYP
1 + 2 OH → **1d** + 2 OH	11.2	8.4	9.7	7.4	8.4	8.5
2 + 2 OH → **2f** + 2 H_2O	−38.7	−101.0	-	−91.6	−88.4	−91.1
3 + 2 OH → **3e** + 2 H_2O	−17.0	−68.4	-	−67.3	−58.8	−61.2
4 + 2 OH → **4f** + H_2O	−64.9	−105.2	-	−113.5	−110.7	−111.7

The reactions observed after the electron transfer are mostly exothermic. An exception is the isomerization of **1** to form **1d**, which is just catalyzed by the electrical current. Hartree–Fock, as usual [18], deviates quite a bit, while the hybrid and double hybrid approaches nicely converge to reasonable results.

3. Conclusions

What do we learn from that? It is obvious that all four bases have a different reactivity. The reactivity of the bases near the cathode is lower than that near the anode. Generally, ring opening reactions are rare. We observe primarily radical reactions at the anode, namely additions and abstractions. In both electrode spaces, direct radical recombination reactions are observed leading to HOOH and H_2, respectively, whereby the latter reaction is dominating at the cathode and is responsible for the low reactivity with the pollutant under these conditions.

The most characteristic reaction in the case of adenine is the cathodic isomerization reaction leading to compound **1d**. This is not in agreement with experiment, where a reduction is described [2]. In view of our limited statistics this discrepancy may be accidental. In the case of cytosine, the anodic dimerization leading to **2f** is the most interesting reaction. At the cathode we observe the formation of **2e**, which is in agreement with the first step of the reaction observed in experiment [3]. In the case of guanine the ring opening reaction leading to **3f** is a remarkable feature. Finally, in the electrolysis of thymine, no characteristic pattern was observed. A cathodic reaction different from the evolution of molecular hydrogen was observed in a single case only.

In view of the surprisingly many different reaction pathways observed, it has to be stated that the investigation of 128 nucleobases in 64 reaction runs is merely a starting point. In contrast to amino acids, where the formation of carbondioxide is predominant, we observe a wide variety of products. This accounts to all four nucleobases. Our simulations give just a crude idea, which must be checked experimentally. The number of runs is limited not only by CPU time but also by the time needed for the evaluation. It is not practical to evaluate several hundred reactive molecular dynamics simulations if the reaction pathway is complex and totally unknown.

We observed little which would answer the original question how one might form harmless or even precious compounds by electrolysis of contaminated water—an exception is of course the cathodic formation of molecular hydrogen. We can contribute, however, a little to the general knowledge about DNA bases: there is nothing which could be identified as a special property or reactivity which would make the four nucleobases the obvious building blocks of the genetic code. On the other hand, these different chemical reactivities might be useful for DNA sequencing using nanodevices [19,20].

4. Methods

Car–Parrinello molecular dynamics simulations [12,13,21] have been performed in the NVE ensemble using the Becke–Lee–Yang–Parr (BLYP) functional in connection with the

Grimme dispersion correction [22]. The time step was chosen as 2 a.u. (0.048 fs) and the fictitious electron mass as 200 a.u. Troullier–Martins pseudopotentials as optimized for the BLYP functional were employed for describing the core electrons [23,24]. The plane-wave cutoff which determines the size of the basis set was set to 70.0 Rydberg. The simulation cell size was $20 \times 20 \times 20$ a.u.^{3} ($10.6 \times 10.6 \times 10.6$ Angstrom^3). Solutions with a density of roughly 1 g/cm^3 were generated and equilibrated for 0.96 ps using the TEMPCONTROL option with the parameters 300 and 100. After equilibration of stable, neutral closed-shell systems, reactive species were generated by removing four protons and four electrons, leading to $OH^{\cdot}$ radicals which simulates the anodic conditions. Alternatively, to simulate cathodic conditions, OH was removed from the solution leading to nascent hydrogen. For the reactive simulations, which took 0.48 ps, the spin-unrestricted version of Kohn–Sham theory was employed [25]. In the production runs, the temperature was not controlled. A total of eight simulations was performed for all four nucleobases, both for the anodic and the cathodic reactions. In every simulation cell, two nucleobases were surrounded by water molecules, hence we have to evaluate the fate of 128 nucleobases.

For comparison, static calculations were performed for the most important reactions using Hartree–Fock, MP2, CCSD, BLYP, B3LYP and B2PLYP with a 6-311G(d,p) basis set as implemented in Gaussian [14–17,26]. For BLYP, B3LYP and B2PLYP a dispersion correction was employed [27].

Supplementary Materials: The following are available at https://www.mdpi.com/article/10.3390/en14165021/s1, Deposited as separate files: cytosine.mpg: Movie of the dimerization of cytosine. cytosine.in3: Input file for CPMD version 4.1.

Author Contributions: Conceptualization, I.F. and E.N.; methodology, I.F.; software, I.F.; validation, I.F. and E N.; formal analysis, I.F.; investigation, I.F.; resources, I.F.; data curation, I.F.; writing—original draft preparation, I.F.; writing—review and editing, E.N.; visualization, I.F.; supervision, I.F.; project administration, I.F. and E.N.; funding acquisition, I.F. and E.N. All authors have read and agreed to the published version of the manuscript.

Funding: This research received no external funding.

Institutional Review Board Statement: Not applicable.

Informed Consent Statement: Not applicable.

Data Availability Statement: A sample input file for CPMD version 4.1 is given in the Supplementary Material. The other 63 input files and the corresponding output files are available on demand from the corresponding author.

Acknowledgments: The study was supported by the Deutsche Forschungsgemeinschaft (DFG), grant FR1246/10-1. Part of the calculations were performed on the local cluster of the Leibniz University of Hannover at the RRZN and on the Höchstleistungsrechner Nord, HLRN, maintained by the North German Supercomputing Alliance, project nic00061.

Conflicts of Interest: The authors declare no conflict of interest.

References

1. Frank, I. Ab-initio molecular dynamics simulation of the electrolysis of waste water. *ChemistrySelect* **2019**, *4*, 4376. [CrossRef]
2. Smith, D.L.; Elving, P.J. Electrochemical Reduction of Purine, Adenine and Related Compounds: Polarography and Macroscale Electrolysis. *J. Am. Chem. Soc.* **1962**, *84*, 1412. [CrossRef]
3. Smith, D.L.; Elving, P.J. Electrochemical Reduction of Pyrimidine, Cytosine and Related Compounds: Polarography and Macroscale Electrolysis. *J. Am. Chem. Soc.* **1962**, *84*, 2741. [CrossRef]
4. Spacek, J.; Fojta, M.; Wang, J. Electrochemical Reduction and Oxidation of Six Natural 2′-Deoxynucleosides at a Pyrolytic Graphite Electrode in the Presence or Absence of Ambient Oxygen. *Electroanalysis* **2019**, *31*, 2057. [CrossRef]
5. Suprun, E.V. Direct electrochemistry of proteins and nucleic acids: The focus on 3D structure. *Electrochem. Commun.* **2021**, *125*, 106983.
6. Hofbauer, F.; Frank, I. Electrolysis of Water in the Diffusion Layer: First-Principles Molecular Dynamics Simulation. *Chem. Eur. J.* **2012**, *18*, 277. [CrossRef]

7. Kiakojouri, A.; Nadimi, E.; Frank, I. Ab-Initio Molecular Dynamics Simulation of Condensed-Phase Reactivity: The Electrolysis of Amino Acids and Peptides. *Molecules* **2020**, *25*, 5414.
8. Blumberger, J.; Bernasconi, L.; Tavernelli, I.; Vuilleumier, R.; Sprik, M. Electronic structure and solvation of copper and silver ions: A theoretical picture of a model aqueous redox reaction. *J. Am. Chem. Soc.* **2004**, *126*, 3928. [CrossRef]
9. Blumberger, J.; Tateyama, Y.; Sprik, M. Ab initio molecular dynamics simulation of redox reactions in solution. *Comput. Phys. Commun.* **2005**, *169*, 256. [CrossRef]
10. Zhang, C.; Sayer, T.; Hutter, J.; Sprik, M. Modeling electrochemical systems with finite field molecular dynamics. *J. Phys. Energy* **2020**, *2*, 032005.
11. Frank, I.; Hutter, J.; Marx, D.; Parrinello, M. Molecular dynamics in low-spin excited states. *J. Chem. Phys.* **1998**, *108*, 4060. [CrossRef]
12. Car, R.; Parrinello, M. Unified Approach for Molecular Dynamics and Density-Functional Theory. *Phys. Rev. Lett.* **1985**, *55*, 2471–2474. [CrossRef] [PubMed]
13. Hutter, J. *CPMD*; Copyright IBM Corp 1990–2015. Copyright MPI für Festkörperforschung Stuttgart 1997–2001. Version 4.1. Available online: http://www.cpmd.org/ (accessed on 24 June 2021).
14. Becke, A. Density-Functional Exchange-Energy Approximation with Correct Asymptotic Behavior. *Phys. Rev. A* **1988**, *38*, 3098–3100. [CrossRef] [PubMed]
15. Becke, A. A New Mixing of Hartree-Fock and Local-Density Functional Theories. *J. Chem. Phys.* **1993**, *98*, 1372–1377. [CrossRef]
16. Grimme, S. Semiempirical hybrid density functional with perturbative second-order correlation. *J. Chem. Phys.* **2006**, *124*, 034108. [CrossRef] [PubMed]
17. Neese, F.; Schwabe, T.; Grimme, S. Analytic derivatives for perturbatively corrected "double hybrid" density functionals: Theory, implementation, and applications. *J. Chem. Phys.* **2007**, *126*, 124115. [CrossRef]
18. Levine, I.N. *Quantum Chemistry*, 5th ed.; Prentice Hall: Upper Saddle River, NJ, USA, 2000.
19. Li, J.; Gershow, M.; Stein, D.; Brandin, E.; Golovchenko, J.A. DNA molecules and configurations in a solid-state nanopore microscope. *Nat. Mater.* **2003**, *2*, 611. [CrossRef]
20. Schneider, G.F.; Kowalczyk, S.W.; Calado, V.E.; Pandraud, G.; Zandbergen, H.W.; Vandersypen, L.M.K.; Dekker, C. DNA Translocation through Graphene Nanopores. *Nano Lett.* **2010**, *10*, 3163. [CrossRef]
21. Marx, D.; Hutter, J. *Ab Initio Molecular Dynamics: Basic Theory and Advanced Methods*; Cambridge University Press: Cambridge, UK, 2009.
22. Grimme, S. Accurate Description of van der Waals Complexes by Density Functional Theory Including Empirical Corrections. *J. Comput. Chem.* **2004**, *25*, 1463. [CrossRef]
23. Troullier, N.; Martins, J.L. Efficient Pseudopotentials for Plane-Wave Calculations. *Phys. Rev. B* **1991**, *43*, 1993. [CrossRef]
24. Boero, M.; Parrinello, M.; Terakura, K.; Weiss, H. Car-Parrinello study of Ziegler-Natta heterogeneous catalysis: Stability and destabilization problems of the active site models. *Mol. Phys.* **2002**, *100*, 2935–2940. [CrossRef]
25. Gunnarsson, O.; Lundqvist, B.I. Exchange and correlation in atoms, molecules, and solids by the spin-density-functional formalism. *Phys. Rev. B* **1976**, *13*, 4274. [CrossRef]
26. Frisch, M.J.; Trucks, G.W.; Schlegel, H.B.; Scuseria, G.E.; Robb, M.A.; Cheeseman, J.R.; Scalmani, G.; Barone, V.; Petersson, G.A.; Nakatsuji, H.; et al. *Gaussian~16 Revision A.03*; Gaussian Inc.: Wallingford, UK, 2016
27. Grimme, S. Semiempirical GGA-type density functional constructed with a long-range dispersion correction. *J. Comput. Chem.* **2006**, *27*, 1787–1799. [CrossRef]